Laminar drag reduction in microchannels using ultrahydrophobic surfaces

Jia Ou, Blair Perot, and Jonathan P. Rothstein
Department of Mechanical and Industrial Engineering, University of Massachusetts, Amherst, Massachusetts 01003-2210

(Received 7 April 2004; accepted 10 September 2004; published online 9 November 2004)

A series of experiments is presented which demonstrate significant drag reduction for the laminar flow of water through microchannels using hydrophobic surfaces with well-defined micron-sized surface roughness. These ultrahydrophobic surfaces are fabricated from silicon wafers using photolithography and are designed to incorporate precise patterns of microposts and microridges which are made hydrophobic through a chemical reaction with an organosilane. An experimental flow cell is used to measure the pressure drop as a function of the flow rate for a series of microchannel geometries and ultrahydrophobic surface designs. Pressure drop reductions up to 40% and apparent slip lengths larger than 20 μm are obtained using ultrahydrophobic surfaces. No drag reduction is observed for smooth hydrophobic surfaces. A confocal surface metrology system was used to measure the deflection of an air–water interface that is formed between microposts and supported by surface tension. This shear-free interface reduces the flow resistance by allowing the fluid to contact only a very small effective area of the silicon surface. The impact of the surface topology on the drag reduction is explored in detail and the results are found to be in good qualitative agreement with the predictions of analytical theory. © *2004 American Institute of Physics*. [DOI: 10.1063/1.1812011]

I. INTRODUCTION

Friction in fluids is manifest by the phenomena of drag—the force required to move an object through a fluid or a fluid through a device. In devices where the fluid flow is laminar and not turbulent, there are currently few demonstrated methods for significantly reducing drag. The development of such a technology could have an enormous economic impact as mechanical technology is miniaturized, microfluidic devices become more widely used, and biomedical analysis moves aggressively towards lab on a chip technologies. In this paper, through a carefully designed set of experiments, we will demonstrate the existence of laminar drag reduction in microchannels having walls fabricated from hydrophobic surfaces with well defined micron-sized roughness.

Water droplets bead on a hydrophobic surface because the chemical composition of the surface tends to repel water molecules resulting in large interfacial tensions.[1] The standard measure of hydrophobicity is the angle that a droplet free-surface makes with the solid that it is resting on. Clean glass is highly hydrophilic and has an equilibrium contact angle with water close to $\theta=0°$.[1] Dimethyldichlorosilane, which is relatively easy to deposit on a surface, has a contact angle with water close to $\theta=100°$.[2] On these and other smooth silanized surfaces, water droplets are typically slightly rounder than hemispherical. Originally inspired by the unique water repellent properties of the lotus leaf,[3] ultrahydrophobic surfaces have recently been developed which are capable of obtaining contact angles with water as high as $\theta=177°$.[2,4–7] These extremely large contact angles result in water droplets that are nearly spherical. In addition, these surfaces have been found to exhibit little or no dynamic contact angle hysteresis between the advancing and receding contact angle.[2,4–7] The difference between a hydrophobic surface and an ultrahydrophobic surface lies not in the surface chemistry, but in the microscale surface roughness. Ultrahydrophobic surfaces are actually very rough with large, micron-sized protrusions coming out of the surface.

It is possible to create ultrahydrophobic surfaces with both regular and irregular patterns of roughness. A scanning electron micrograph of an ultrahydrophobic plasma etched polypropylene surface and an optical micrograph of an ultrahydrophobic lithographically etched silicon surface are shown in Fig. 1. The equilibrium contact angles for each of these surfaces were found to be greater than $\theta>160°$. Öner and McCarthy[4] performed a detailed experimental study of the effect of surface roughness on ultrahydrophobic behavior using lithographically etched silicon surfaces chemically modified by a series of organosilanes. The silicon surfaces were patterned with regular arrays of microposts and the receding, and advancing contact angles were measured as the cross sectional geometry, height, and spacing of the microposts were systematically varied. The results of Öner and McCarthy[4] show that for microposts between 10 μm to 40 μm across, the contact angle is nearly independent of cross sectional geometry, post height (only heights greater than 20 μm were tested), and the surface chemistry. However, Öner and McCarthy[4] found that a significant deterioration of the ultrahydrophobic properties of the surface occur as the spacing between microposts is increased beyond about 64 μm.

Chen *et al.*[2] demonstrated that the topological nature of the rough surface and the resulting lack of continuity in the three phase contact line is critically important for determine the degree of hydrophobicity of a surface. The hydrophobicity of the microscale surface roughness prevents the water

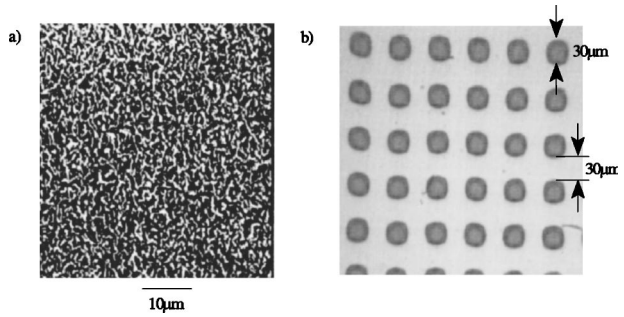

FIG. 1. Examples of ultrahydrophobic surfaces. Included are (a) a plasma-etched polypropylene surface and (b) a lithographically etched silicon surface patterned with 30 μm tall cubic microposts.

from moving into the pores between the peaks of the microposts. Instead of wetting the surface, the water stands off, touching only as many microposts as necessary to support the free surface in between.[3] The resulting contorted, discontinuous contact line becomes destabilized, jumping from one micropost to the next, nearly eliminating contact angle hysteresis. A schematic diagram of this physical model is shown in Fig. 2. Using Young's law and assuming an average spacing between posts of w, one can show that a pressure difference of

$$\Delta p = p_w - p_a = 4\gamma/w \cos(\pi - \phi) \tag{1}$$

can be supported by the air–water interface.[8] The angle ϕ dynamically adjusts to balance the pressure within the water until the contact angle between the water and the ultrahydrophobic surface θ is reached. Beyond this pressure, the water will advance into the gap, compressing or displacing the air trapped between the microscale protrusions and affecting the ultrahydrophobic nature of the surface. Evidence of such a loss of the air–water interface can be seen in the experiments of Öner and McCarthy[4] as the spacing between microposts was systematically increased.

The lack of contact angle hysteresis makes the drop unstable to even the smallest perturbation and allows it to move very easily across these surfaces.[2,5] This can be seen

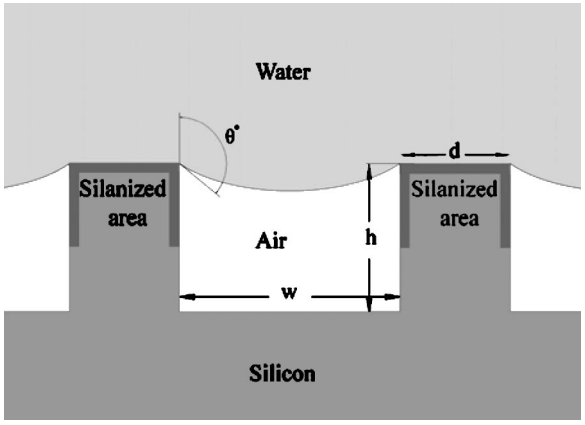

FIG. 2. Schematic diagram of a model for ultrahydrophobic drag reduction. A combination of surface hydrophobicity and roughness combine to allow water to stand way from the solid surface.

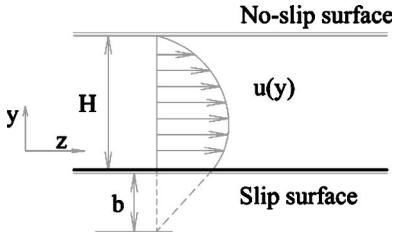

FIG. 3. Schematic diagram defining the slip length and slip velocity at a solid–liquid interface.

explicitly if one calculates the critical line force per unit length of the perimeter required to start a drop moving over a solid surface[9]

$$F = \gamma_{LV}(\cos\ \theta_R - \cos\ \theta_A), \tag{2}$$

where θ_A is the advancing contact angle, θ_R is the receding contact angle, and γ_{LV} is the surface tension of the water. Kim and Kim[10] experimentally studied the flow resistance of water drops sliding down inclined surfaces in both open and confined channels geometries. The channels were fabricated out of ultrahydrophobic silicon surfaces with both micropost and nanopost patterns. Measurements of the minimum inclination angle required to initiate flow demonstrated drag reductions of 60% for the micropost patterns and 99% for the nanopost patterns.[10] The observed drag reductions were found to correlate directly to the contact angle hysteresis of the surfaces as demonstrated by Eq. (2). The question to be addressed by our research is whether ultrahydrophobic surfaces can similarly reduce drag in laminar flow through a microchannel in the absence of a contact line.

The no-slip condition is almost universally accepted as the proper boundary condition to impose on a solid–liquid interface. In actuality, no-slip is an accurate approximation only at macroscopic length scales. For reasons that can be largely explained by molecular chemistry, fluids actually do slip at a wall. However, the slip effect is on the order of molecular sizes and is only important in devices that operate at extremely small length scales. The concept of a slip boundary condition was first proposed by Navier[11] and is shown schematically in Fig. 3. In Navier's model, the slip velocity $u_{z,0}$ is proportional to the shear rate experienced by the fluid at the wall

$$u_{z,0} = b(\partial u_z/\partial y), \tag{3}$$

where b is the slip length. For a finite value of b, a slip velocity exists at the wall. For flows of entangled polymer solutions and melts, large slip lengths of $b > 100$ μm have been reported.[12,13] However, for the flow of simple fluids such as pure water past hydrophobic smooth surfaces, much smaller slip lengths have been observed.[14–21] Zhu and Granick[21] used a surface forces apparatus whose mica crystal surfaces were modified with methyl-terminated self-assembled organic monolayers making them hydrophobic to measure slip lengths using both water and tetradecane. A periodic squeezing flow with nanometer size oscillations was used to measure the hydrodynamic forces and calculate the resulting slip length as a function of oscillation frequency

and amplitude, surface roughness, and contact angle for a series of different fluids.[21,22] In their experiments, slip lengths of between 0 nm $< b <$ 40 nm with the maximum slip lengths corresponding to the surfaces with the smallest RMS roughness. This apparent slip is thought to be the result of dissolved gas bubble or films coming out of solution near the interface thereby reducing the fluid viscosity in close proximity to the wall and giving the appearance of a failure of the no-slip condition.[21,23]

In laminar flows, the effect of slip only becomes important in macroscopic flows when the slip length is comparable to the length scale of the flow geometry. Using the Navier slip boundary condition, the volume flow rate per unit length q of fluid between the two infinite parallel plates separated by a height H can be expressed as a function of the viscosity μ, the pressure gradient dp/dx, and the slip length

$$q = \frac{H^3}{4\mu}\left(-\frac{dp}{dz}\right)\left[\frac{1}{3} + \frac{b}{H}\right]. \tag{4}$$

A 20% decrease in the drag requires a slip length of $b = h/15$. Thus, for a simple fluid flowing over a smooth hydrophobic surface, where $b < 40$ nm, a significant drag reduction should only be observed for flow geometries smaller than $h < 600$ nm. The results of prior studies[14] and our current experiments using ultrahydrophobic surfaces in microchannels have demonstrated that ultrahydrophobic surfaces can achieve a significant drag reduction at considerably larger length scales. This suggests that an entirely different slip mechanism is present at these surfaces which our experiments confirm relies on *both* hydrophobicity and surface roughness. We will demonstrate that laminar drag reduction is achieved through the reduced effective surface area of the solid in contact with the flowing fluid. The boundary condition for the fluid in contact with the micropost remains no-slip, however, the air–water interfaces supported between microposts is shear free and cannot resist the flow. By decreasing the size of the microposts and/or increasing the separation between them we will quantitatively demonstrate that it is possible to reduce flow resistance and generate significant laminar drag reduction in agreement with this model.

Watanabe *et al.*[14] investigated the flow of water through 6 mm and 12 mm diameter circular pipes having highly water repellent walls. The walls of the pipes were coated with a fluorine alkane modified acrylic resin resulting in a porous hydrophobic surface crisscrossed by 10 μm to 20 μm wide microcracks. Pressure drop and velocity profile measurements demonstrated drag reduction up to 14% and slip lengths up to 450 μm for flows with Reynolds numbers between $500 < \mathrm{Re} < 10\,000$.[14,24] Here the Reynolds number is defined as $\mathrm{Re} = \rho U D_H/\mu$, where ρ is the density of the fluid, $U = Q/A$ is the average velocity, Q is the volume flow rate, A is the cross sectional area of the channel, $D_H = 4A/P$ is the hydraulic diameter, and P is the perimeter of the channel. Watanabe *et al.*[14] hypothesized that one possible explanation for the drag reduction observed in their pipes was the formation of a free surface above the air-filled microcracks. In the experiments presented in this paper we will present definitive proof of the presence of a shear-free air–water interface through direct measurements of the surface deflection. In addition, using lithographically etched silanized silicon surfaces the microsurface topology can be precisely controlled allowing us to systematically investigate the affect of topological changes on drag reduction and to compare our experimental measurements directly to both the analytical solutions of Philip,[25,26] Lauga and Stone,[27] and numerical simulations. The results presented in this paper will strongly support the theory that ultrahydrophobic drag reduction is due to reduced effective contact area between the fluid and the surface.

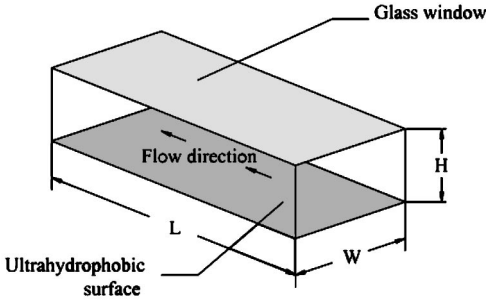

FIG. 4. Schematic diagram of the experimental microchannel flow cell including the important physical dimensions.

The outline of this paper is as follows. In Sec. II, we describe the experimental setup and the fabrication of the ultrahydrophobic surfaces. In Sec. III, we present our experimental results demonstrating significant laminar drag reduction. Finally, in Sec. IV we conclude.

II. EXPERIMENT

A. General procedures

The experimental flow cell shown in Fig. 4 was designed and fabricated to measure the pressure drop resulting from the laminar flow of water through a rectangular microchannel. A series of rectangular cross section microchannels with a thickness between 76 μm $< H <$ 254 μm were precisely machined from plastic. As the thickness of the microchannels was changed, the aspect ratio of each microchannel was held fixed at $\alpha = W/H = 20$ and the overall length of the microchannel was $L = 50$ mm. A smooth hydrophilic piece of glass was used as the upper wall of the microchannel to allow for optical access to the flow. The glass plate was glued on an aluminum frame and mounted inside an aluminum superstructure. The plastic microchannels were precisely positioned and tightly clamped between the slide glass and the lower wall of the microchannel to make a well sealed flow cell. The lower wall of the microchannel was designed to be easily interchangeable making it possible to perform drag reduction measurements on a host of different surfaces including a series of ultrahydrophobic silicon wafers with a prescribed surface roughness pattern and smooth hydrophobic silicon wafers.

An inlet and outlet were machined into the glass cover slip. A syringe pump (Model 100, KD Scientific Inc.) was used to drive the fluid through the microchannel with flow rates between 0.03 mm^3/s and 115 mm^3/s. The pressure drop was measured using a manometer with a resolution of

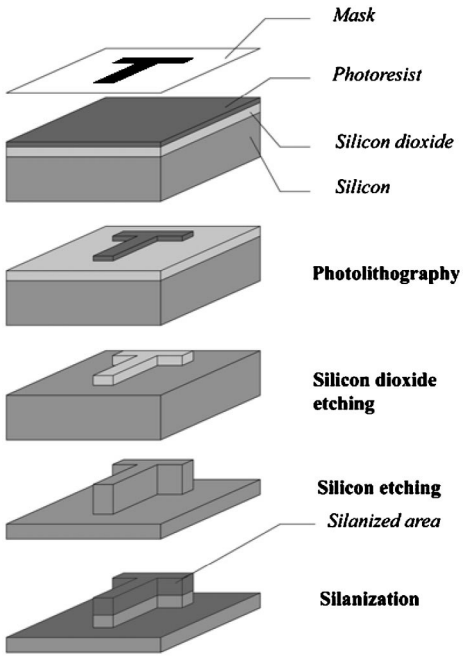

FIG. 5. Schematic diagram outlining the procedure for creating of ultrahydrophobic surfaces.

0.25 mm or 2.5 Pa. This resolution was more than adequate for the desired pressure drop measurement. The opening for the manometer was positioned far enough downstream of the inlet for the flow to be fully developed and to avoid entrance effects.[8] For all of the experimental measurements reported in the following sections, the Reynolds number based on the hydraulic diameter was less than $\mathrm{Re}<1000$ and thus the flows were all laminar.[8]

B. Preparation of ultrahydrophobic silicon surfaces

Photolithography and wet etching have been used in semiconductor industry for years for patterning silicon, glass, or gallium arsenide surfaces.[28,29] In recent years, these techniques have been modified and adapted for fabrication of microfluidic devices.[30,31] In order to fabricate the ultrahydrophobic surfaces, standard photolithographic techniques were used to precisely and reproducibly control the size, height, spacing, and geometry of the micron scale roughness designed onto silicon wafers. A schematic diagram outlining the fabrication procedure of ultrahydrophobic surfaces is shown in Fig. 5.

First, AutoCAD™ was used to design the size, spacing, and alignment of the desired micropatterned surface. The computer-aided design drawing was then printed on a high resolution transparency at 5080 dpi. At this resolution, features between 20–30 μm were easily produced. The transparency served as a mask for contact photolithography using a positive photoresist on a silicon wafer.[30] A silicon dioxide layer with a thickness of 0.3 μm was grown on the surface of silicon wafer (100 Orientation, International Wafer Service Inc., CA). A uniform layer of positive photoresist (S1813 MICROPOSIT™ Photoresist, Shipley Co.) was then coated on both sides of the silicon wafer using a spin coater (Headway Research Inc.). The mask was aligned with the wafer's crystal structure direction and a high-strength ultraviolet light source was used to expose the photoresist (model 100UV30S1, Karlsus Inc.). The unexposed photoresist was dissolved in a solution of Microposit 351 developer (J. T. Baker Co.) with water in a 1:4 ratio.

The area of silicon dioxide surface not protected by the photoresist was etched with a buffered oxide etch solution (BOE) (J. T. Baker Co.) of 10% hydrofluoric acid in water. According to the isotropic property of the silicon dioxide, the etching is nondirectional. The resulting pattern in the silicon dioxide after the BOE can therefore be slightly different from the original mask. The remaining silicon dioxide protects the underlying silicon from the silicon etchant (PSE-300, Transene Co. Inc. MA). The etchant was heated to its boiling temperature, 115°C, for the duration of the etching process. A custom-built glass container was designed to condense and recollect the vapor of the boiling etchant. On the bottom of the container, nitrogen was fed into the etchant to produce a constant current in the container, transporting the oxide away from the wafer surface, while ensuring a uniform etchant concentration near the wafer and therefore a uniform feature depth across the wafer. The amount of material removed was controlled through modification of the etching time. The depth of the microstructure was measured using a surface profilometer and the desired pattern confirmed using both optical and electron microscopy.

Once the desired roughness was imparted on the silicon wafer, it was reacted with a silanizing agent to make it ultrahydrophobic. Öner and McCarthy[4] found that the contact angle of water could be maximized and the contact angle hysteresis minimized by reacting the silicon surfaces with heptadecafluoro-1,1,2,2-tetrahydrodecyldimethylchlorosilane (Gelest Inc.) in the vapor-phase (65–70°C).[4] After completion of the reaction, the ultrahydrophobic surfaces were found to have equilibrium contact angle with water of between $130°<\theta_{eq}<174°$ and demonstrated little contact angle hysteresis. As a specific example, the surface shown in Fig. 6(c), which contains a regular array of $d=30$ μm square microposts with a spacing between microposts of $w=15$ μm was found to have advancing/receding contact angles of $\theta_a/\theta_r=162°/137°$. For comparison, the advancing/receding contact angles of the smooth silanized silicon surface seen in Fig. 6(b) was measured and found to be $\theta_a/\theta_r=118°/100°$.

III. RESULTS AND DISCUSSION

A series of experiments were performed to demonstrate laminar drag reduction using ultrahydrophobic surface over a wide range of flow rates. The effects of channel height, micropost and microridge spacing size, and height were systematically investigated to optimize the observed drag reduction. In Fig. 6, the experimental measurement of pressure drop through a rectangular microchannel having dimensions of width of $W=2.54$ mm, thickness $H=127$ μm, and length $L=50$ mm are shown for a series of hydrophobic and ultrahydrophobic surfaces. The experimental pressure drop measurements across the smooth silanized silicon surface are

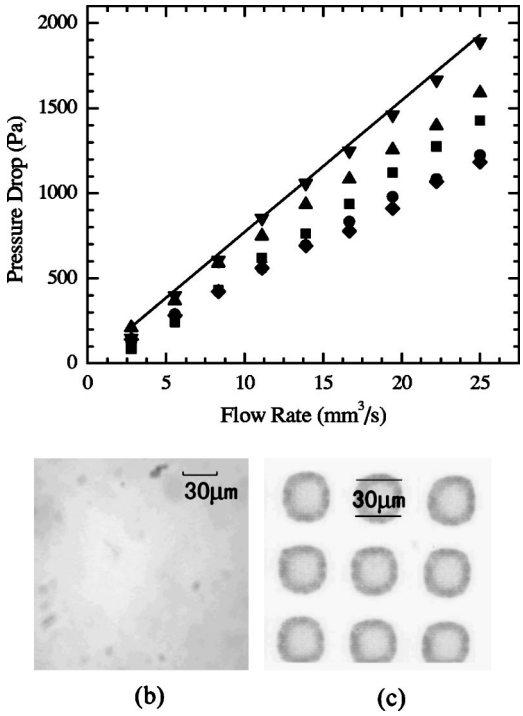

FIG. 6. Pressure drop measurements as a function of flow rate for a series of different hydrophobic and ultrahydrophobic surfaces in a microchannel having dimensions $W=2.54$ mm, $H=127$ μm, and $L=50$ mm. The experimental data in (a) include theoretical pressure drop calculation (—), a smooth hydrophobic silicon surface (▼), and a series of ultrahydrophobic surfaces with a regular array of $d=30$ μm square microposts with a spacing between microposts of $w=15$ μm (▲), $d=30$ μm and $w=30$ μm (■), $d=30$ μm and $w=60$ μm (●), and $d=30$ μm and $w=150$ μm (♦). Optical micrographs of the smooth hydrophobic surface and the ultrahydrophobic surface with $d=30$ μm and $w=30$ μm can be found in (b) and (c), respectively.

found to agree well with the theoretical predictions over a wide range of flow rates. For a rectangular channel with aspect ratio of $\alpha=20$, and no-slip boundary conditions, the pressure drop can be calculated from the friction factor[32]

$$f=\frac{\Delta p}{(L/D_H)}\frac{1}{1/2\rho U^2}=\frac{92}{\mathrm{Re}}. \tag{5}$$

The friction factor for flow between two infinite plates is $f=96/\mathrm{Re}$.[32] The agreement between the smooth hydrophobic surface and the theory demonstrate that the no-slip boundary condition holds and thus confirms both the quality of our microchannel flow cell design and the accuracy of the pressure drop measurement. These measurements also demonstrate the limitations of this technique for measuring slip lengths. Starting from Eqs. (4) and (5), the slip length can be approximated directly from measurements of pressure drop and volume flow rate

$$b=\frac{23\mu Q}{6WH^2}\left(-\frac{dp}{dz}\right)^{-1}-\frac{H}{3}. \tag{6}$$

The minimum corresponding slip length that can be measured in our system is thus a function of the geometry, the flow rate, and the precision of the pressure drop measurements. For the experiments shown in Fig. 6, the minimum measurable slip length is approximately $b_{min}\approx 1$ μm.

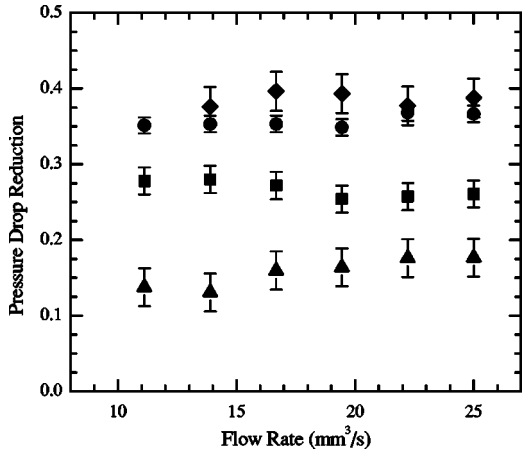

FIG. 7. Average pressure drop reduction as a function of flow rate for a series of different surfaces in a microchannel having dimensions $W=2.54$ mm, $H=127$ μm, and $L=50$ mm. The experimental data in (a) include a series of ultrahydrophobic surfaces with a regular array of square micropost with $d=30$ μm square microposts with a spacing between microposts of $w=15$ μm (▲), $d=30$ μm and $w=30$ μm (■), $d=30$ μm and $w=60$ μm (●), and $d=30$ μm and $w=150$ μm (♦).

The ultrahydrophobic surfaces used in the experiments presented in Fig. 6 consisted of 30 μm square microposts in a regular array. The spacing between the microposts was systematically increased from $w=15$ μm to 30 μm to 60 μm and finally to 150 μm to investigate role of micropost spacing and the shear-free air–water interface on drag reduction. In each case, the pressure drop was found to increase linearly with flow rate. For all of the ultrahydrophobic surfaces tested, the pressure drop was found to be significantly smaller than the smooth silanized silicon surface and the prediction of theory where the no-slip boundary condition is applied to both of the channel surfaces. The magnitude of the reduction in the pressure drop was found to increase monotonically with increasing spacing between microposts.

To highlight the magnitude of the pressure drop reduction observed in Fig. 6, the data are recast in term of a dimensionless pressure drop reduction

$$\Pi=\frac{\Delta p_{no\text{-}slip}-\Delta p}{\Delta p_{no\text{-}slip}}, \tag{7}$$

where Δp is the experimentally measured pressure drop and $\Delta p_{\text{no-slip}}$ is the theoretical pressure drop prediction for flow over a no-slip surface at the same flow rate. In Fig. 7, the dimensionless pressure drop reduction is plotted as a function of flow rate for all the surfaces shown in Fig. 6. As a direct result of the linear growth of the pressure drop observed in Fig. 6, the pressure drop reduction calculated from Eq. (7) was found to be constant over all of the experimentally imposed flow rates for each ultrahydrophobic surface tested. Therefore, in future figures, a pressure drop reduction averaged over a wide range of flow rates will be presented, allowing for the direct comparison between ultrahydrophobic surfaces with different micropost sizes and spacing, and channel geometries.

If a shear-free air–water interface exists and is supported between the hydrophobic microposts, then the increase in

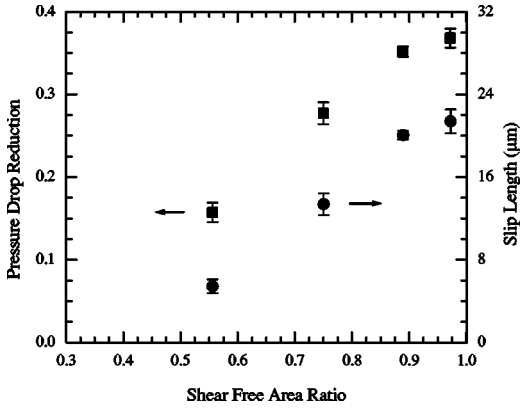

FIG. 8. Average pressure drop reduction (■) and slip length (●) as a function of shear-free surface area ratio for the flow past a series of different of ultrahydrophobic surfaces with a regular array of $d=30$ μm square microposts with variable spacing in a microchannel having dimensions $W=2.54$ mm, $H=127$ μm, and $L=50$ mm.

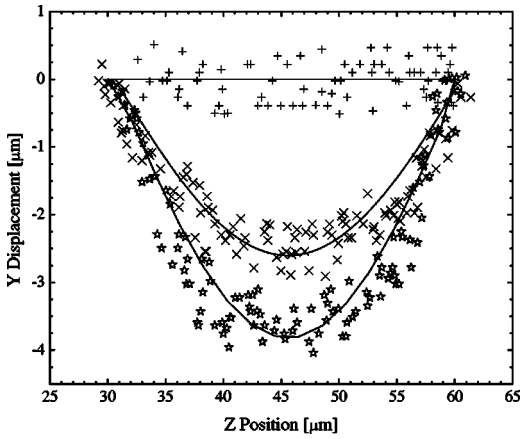

FIG. 9. Experimentally measured of the air–water interface profile suspended between microposts spaced $w=30$ μm apart. The data include from top to bottom: the interface profile for the no flow condition; a flow rate of $Q=300$ ml/hr and a pressure drop of $\Delta p=3200$ Pa; and $Q=420$ ml/h and $\Delta p=4500$ Pa. Superimposed over the data are fits to the theoretical interface profile in Eq. (9).

pressure drop reduction is a direct result of the increased shear-free air–water interface surface area or alternatively a reduction in the no-slip surface area formed by the top of the microposts. For each of the ultrahydrophobic surfaces presented in Figs. 6 and 7, an average pressure drop reduction was calculated over all the experimental flow rates and plotted in Fig. 8 as a function of the shear-free area ratio defined as

$$\beta = \frac{A_{total} - A_{no\text{-}slip}}{A_{total}}. \tag{8}$$

Here, A_{total} is the total area of the ultrahydrophobic surface and $A_{\text{no-slip}}$ is the area of the top of the microposts where the no-slip boundary condition holds. In the limit that $H \gg h$, the shear-free area ratio reduces to $\beta = 1 - H^2/h^2$ and one would expect the pressure drop reduction to increase as $\Pi \propto H^2$. This scaling is indeed reflected in the data. The data in Fig. 8 show a linear dependence of the pressure drop reduction on the shear-free area ratio at moderate values of the shear-free area ratio and appears to plateau to a value of $\Pi = 0.37$ as $\beta \to 1$. Also shown in Fig. 8 are the slip lengths calculated from Eq. (6). The slip lengths were observed to increase with increasing micropost spacing and slip lengths as large $b=21$ μm were calculated for the $d=30$ μm square microposts spaced $w=150$ μm apart.

To confirm the hypothesis of the existence of a shear-free air–water interface supported between the hydrophobic microposts, a confocal surface metrology system (model LT-8010, Keyence Corp.) was used to obtain the profile of the interface. The system combines the principles of confocal microscopy[33] with a dynamic focus-detection technique.[34] Like conventional confocal microscopy, a laser beam is passes through a semi-silvered mirror and is focused on a target surface using high numerical aperture optics. The reflections from that surface are then passed through a pinhole and collected on a photodetector. In a confocal surface metrology system, an active tuning fork is used to rapidly oscillate the objective lens up and down. By determining the location of the objective lens when the reflection off of a surface is in focus, the height and profile of a reflective surface can be measured. This confocal surface metrology system has the ability to measure the position of several surfaces simultaneously making differential height measurements possible. According to the manufacturer, the confocal surface metrology system has a 7 μm diameter laser spot and a vertical resolution of 0.1 μm, however, our calibration tests have shown that the resolution of the system is closer to 0.5 μm.

The profile of the air–water interface was acquired by determining the difference in the heights measured from the reflection from the water–glass interface at the top of the channel and the air–water interface between the microposts. The measurements were taken at the midpoint of the microchannel ($z=25$ mm) and an automated XY stage (model ZETA4, Compumotor) was used to step the laser between the center of adjacent microposts in the flow direction. The resulting measurements of the free-surface curvature for a se-

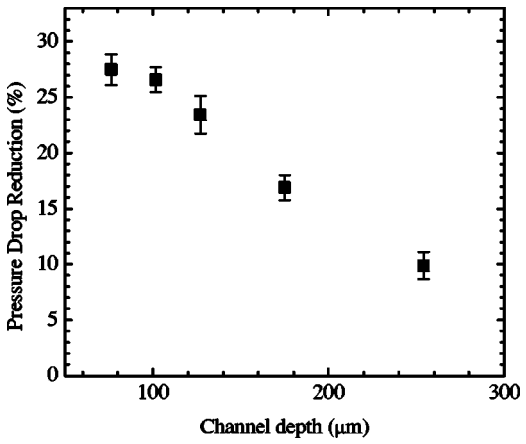

FIG. 10. Average pressure drop reduction as a function of channel depth for the flow through a rectangular channel of length $L=50$ mm and aspect ratio $\alpha=20$ using an ultrahydrophobic surface with a regular array of square micropost having $d=30$ μm and $w=30$ μm.

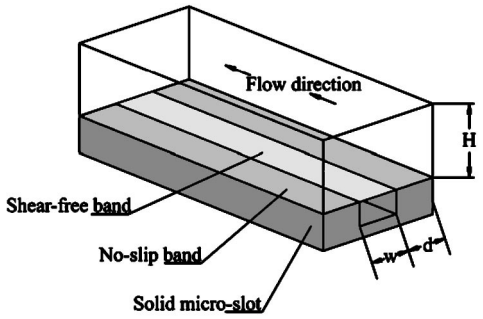

FIG. 11. Schematic diagram of the Stokes flow problem solved by Philip (Refs. 25 and 26).

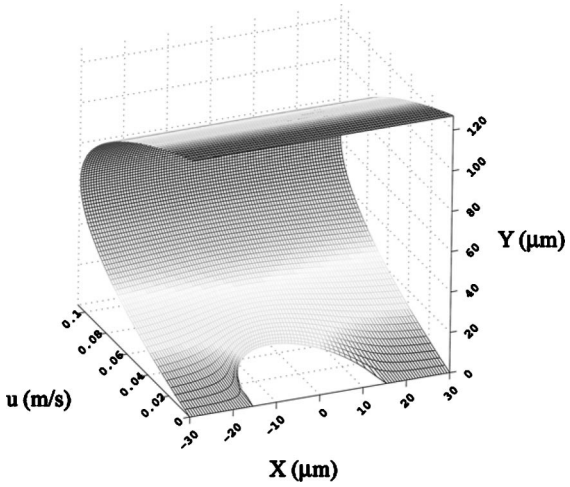

FIG. 12. Velocity profile resulting from the analytical solution of Philip (Refs. 25 and 26) [Eq. (9)] for a microchannel with a height of $H=127$ μm, a shear-free band of width $w=30$ μm and a pressure gradient of $-dp/dz=25$ kPa/m.

ries of increasing flow rate (and thus pressure drops) are shown in Fig. 9 for an ultrahydrophobic surface with a regular array of $d=30$ μm square microposts set $w=30$ μm apart. Because the magnitude of the free-surface deflection measurements is close to the vertical resolution of the system, the data contain some noise, however, these measurements clearly demonstrate the existence of an air–water interface between the microposts. Even in the presence of flow, the curvature of the free surface remains roughly symmetric and the maximum deflection is found to increase nearly linearly with the applied pressure.

Because the measurements were taken between the midpoints of adjacent microposts, the deflection in the free surface $\delta(z)$ can be approximated by the deflection of an elastic beam under a uniformly distributed load[35]

$$\delta(x) = \alpha(z^4 - 2wz^3 + w^3 z). \tag{9}$$

The coefficient of proportionality α is among other things a linear function of the local pressure. A best fit of Eq. (9) to each of the data sets is presented in Fig. 9 and demonstrates a good quantitative fit to the data.

The effect of channel height on laminar drag reduction and slip length was also investigated. The pressure drop was measured as a function of volume flow rate for a series of different channel heights varying from $H=76.2$ μm to 254 μm. In all cases, the aspect ratio was held fixed at $\alpha=20$ to minimize possible discrepancies in the data which might arise from end effects in the channel. An average pressure drop reduction over a range of flow rates was calculated for an ultrahydrophobic surface having a regular array of $d=30$ μm square microposts with $w=30$ μm spacing and plotted in Fig. 10 as a function of channel height. Pressure drop reductions as large as $\Pi=0.35$ were observed and the pressure drop reduction was found to decrease linearly with increasing channel height. These observations were consistent for all the ultrahydrophobic surfaces tested and agree well with the analytical results of both Lauga and Stone[27] and Philip.[25,26]

Philip[25,26] derived an analytical solution to Stokes flow in an infinite channel where, as shown in Fig. 11, one wall is no-slip while the other wall contains a shear-free band of width w running parallel to the flow direction. Philip[25,26] demonstrated that the velocity profile in the flow can be expressed as the following:

$$u_z(x,y) = \frac{H^2}{2\mu}\left(-\frac{\partial p}{\partial z}\right)\left\{\frac{y}{H}\left(1-\frac{y}{H}\right) + \frac{2}{\pi}\mathrm{Im}\left[\cosh^{-1}\left(\frac{\cosh\left(\frac{\pi}{2}\frac{x+iy}{H}\right)}{\cosh\left(\frac{\pi}{4}\frac{w}{H}\right)}\right) - \frac{\pi}{2}\frac{x+iy}{H}\right]\right\}. \tag{10}$$

The velocity profile resulting from Eq. (9) is plotted in Fig. 12 for a microchannel with a height of $H=127$ μm, a shear-free band of width $w=30$ μm, and a pressure gradient of $-dp/dz=25$ kPa/m. As seen in Fig. 12, the increase in the fluid velocity in the vicinity of the shear-free band is significant, but its influence on the flow decays quickly with increasing distance from the wall. To compare the Philip model directly to our experimental measurements, a series of ultrahydrophobic surfaces were fabricated with microridge patterns like those shown in Fig. 13. The widths of the microridges were varied from $d=20$ to 30 μm and the spacing between ridges was varied from $w=20$ to 80 μm. The experimental measurements of pressure drop reduction are plotted in Fig. 14 as a function of channel height. In order to calculate the pressure drop reduction predicted by the Philip model, Eq. (9) was numerically integrated across the channel and from the center of one microridge to the next and multiplied by the number of shear-free bands N to determine the volume flow rate for a series of different pressure drops and microridge spacings and sizes,

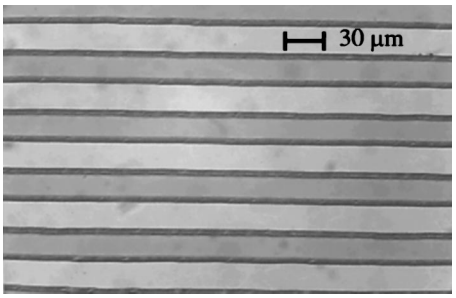

FIG. 13. Micrograph of an ultrahydrophobic surface with microridges etched onto a silicon wafer.

$$Q = N\frac{H^2}{2\mu}\left(-\frac{\partial p}{\partial z}\right)\int_{-1/2(w+d)}^{1/2(w+d)}\int_0^H\left\{\frac{y}{H}\left(1-\frac{y}{H}\right)\right.$$
$$+\frac{2}{\pi}\mathrm{Im}\left[\cosh^{-1}\left(\frac{\cosh\left(\frac{\pi}{2}\frac{x+iy}{H}\right)}{\cosh\left(\frac{\pi}{4}\frac{w}{H}\right)}\right)\right.$$
$$\left.\left.-\frac{\pi}{2}\frac{x+iy}{H}\right]\right\}dy\,dx. \qquad (11)$$

In Fig. 14, the predictions of the Philip model are superimposed over the experimental data. The model qualitatively captures the trend in the data, but systematically underpredicts the magnitude of the pressure drop reduction. The errors originate from the comparison of Philip's analytical solution to the flow over a single shear-free band in an infinite no-slip surface to the flow over a periodic array of shear-free bands. In the limit that $w \gg d$, Eq. (10) should be a good approximation. For all other cases, Eq. (10) will systematically underpredict the velocity of the flow directly above the microridges and thus the pressure drop reduction as seen in Fig. 14.

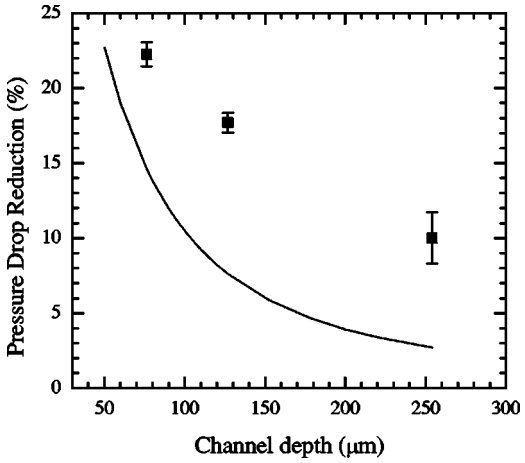

FIG. 14. Pressure drop reduction as a function of channel depth for the flow through a microchannel with an aspect ratio of $\alpha=20$ and a length of $L=50$ mm past an ultrahydrophobic surface with $d=30$ μm wide microridges spaced $w=30$ μm apart (■). Also included is the prediction of the analytical solution by Philip (Refs. 25 and 26) (—).

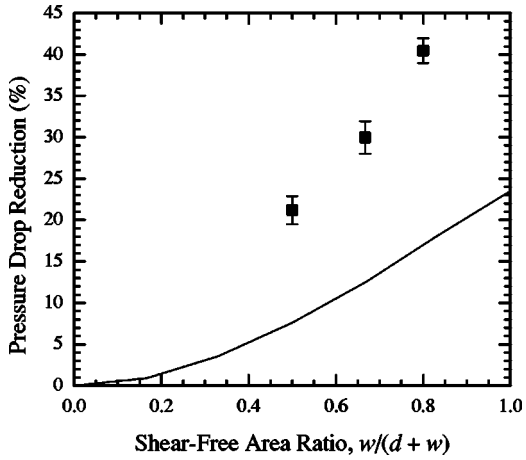

FIG. 15. Pressure drop reduction as a function of microridge spacing for the flow through a microchannel having dimensions $W=2.54$ mm, $H=127$ μm, and $L=50$ mm past an ultrahydrophobic surface with $d=20$ μm wide microridges spaced $w=20$ μm, 40 μm, and 80 μm apart (■). Also included is the prediction of the analytical solution by Philip (Refs. 25 and 26) (—).

In Fig. 15, the microchannel dimensions were held fixed at $W=2.54$ mm, $H=127$ μm, and $L=50$ mm and the spacing between the $d=20$ μm wide microridges was varied from $w=20$ μm to 40 μm to 80 μm. The resulting pressure drop reduction is plotted as a function of dimensionless microridge spacing, $\beta=d/(d+w)$, in Fig. 15. The dimensionless microridge spacing is equivalent to the shear-free area ratio. The pressure drop reduction was found to increase monotonically with increasing microridge spacing. Pressure drop reductions larger than $\Pi>40\%$ corresponding to a slip length of over $b>24$ μm were observed as the shear-free area ratio approached unity. Again, the trends in the data are well matched by the predictions of analytical solution of Philip,[25,26] however, the magnitude of the experimentally obtained pressure drop reduction is underpredicted as it was in Fig. 14. If we now compare the drag reduction characteristics of ultrahydrophobic surfaces with microridges to those with microposts, we find that for the same microchannel geometries and shear-free area ratios, microridges aligned in the flow direction consistently out perform regular arrays of square microposts. Thus, the precise pattern of surface roughness plays a significant role in optimization of the laminar drag reduction achieved through the use of ultrahydrophobic surfaces.

IV. CONCLUSIONS

In this paper, we have shown through a carefully designed set of experiments that laminar drag reduction in microchannels is possible when the walls of the microchannel are fabricated from hydrophobic surfaces with well-defined micron-sized roughness. The combination of microscale roughness and hydrophobicity result in a shear-free air–water interface supported by the surface tension of the water thereby trapping air between the microposts. The existence

and deflection of this air–water interface under flow conditions was obtained using a confocal surface metrology system. The presence of the air–water interface and the resulting shear-free boundary condition results in pressure drop reductions of over 40% and apparent slip lengths exceeding 20 μm. The effectiveness of these surfaces was found to increase with increasing roughness spacing and decreasing channel height. Two different roughness patterns were tested, microposts and microridges. The resulting pressure drop reductions and slip lengths obtained with the ultrahydrophobic surface with microridges were compared directly to the analytical Stokes flow solution of Philip.[10] The agreement between the experiments and the analytical solution were qualitatively quite good.

ACKNOWLEDGMENTS

The authors would like to thank Thomas McCarthy and John Nicholson of the University of Massachusetts for their assistance fabricating the ultrahydrophobic surfaces and Pirouz Kavehpour of UCLA for his assistance with the confocal surface metrology measurements. This research was partially supported by the Air Force Office of Scientific Research (Grant No. F49620-00-1-0033) and 3M through a Non-Tenured Faculty Award.

[1] J. N. Israelachvili, *Intermolecular and Surface Forces: With Applications to Colloidal and Biological Systems* (Academic, London, 1985).
[2] W. Chen, A. Y. Fadeev, M. C. Hsieh, D. Öner, J. P. Youngblood, and T. J. McCarthy, "Ultrahydrophobic and ultralyophobic surfaces: some comments and examples," Langmuir **15**, 3395 (1999).
[3] W. Barthlott and C. Neinhuis, "Purity of the sacred lotus, or escape from contamination in biological surfaces," Planta **202**, 1 (1997).
[4] D. Öner and T. J. McCarthy, "Ultrahydrophobic surfaces. Effects of topography length scales on wettability," Langmuir **16**, 7777 (2000).
[5] J. Bico, C. Marzolin, and D. Quere, "Pearl drops," Europhys. Lett. **47**, 220 (1999).
[6] J. P. Youngblood and T. J. McCarthy, "Ultrahydrophobic polymer surfaces prepared by simultaneous ablation of polypropylene and sputtering of poly(tetrafluorethylene) using radio frequency plasma," Macromolecules **32**, 6800 (1999).
[7] A. Y. Fadeev and T. J. McCarthy, "Trialkylsilane monolayers covalently attached to silicon surfaces: Wettability studies indicating that molecular topography contributes to contact angle hysteresis," Langmuir **15**, 3759 (1999).
[8] F. M. White, *Fluid Mechanics* (McGraw-Hill, New York, 2003).
[9] E. Wolfram and R. Faust, in *Wetting, Spreading and Adhesion*, edited by J. F. Padday (Academic, New York, 1978).
[10] J. Kim and C.-J. Kim, Proceedings of the IEEE Conference MEMS, Las Vegas, NV, 2002.
[11] S. Goldstein and Aeronautical Research Council (Great Britain), *Modern Developments in Fluid Dynamics; An Account of Theory and Experiment Relating to Boundary Layers, Turbulent Motion and Wakes* (Dover, New York, 1965).
[12] V. Mhetar and L. A. Archer, "Slip in entangled polymer melts. 1. General features," Macromolecules **31**, 8607 (1998).
[13] V. Mhetar and L. A. Archer, "Slip in entangled polymer solutions," Macromolecules **31**, 6639 (1998).
[14] K. Watanabe, Yanuar and H. Udagawa, "Drag reduction of Newtonian fluid in a circular pipe with highly water-repellent wall," J. Fluid Mech. **381**, 225 (1999).
[15] E. Schnell, "Slippage of water over nonwettable surfaces," J. Appl. Phys. **27**, 1149 (1956).
[16] R. Pit, H. Hervet, and L. Leger, "Friction and slip of a simple liquid at a solid surface," Tribol. Lett. **7**, 147 (1999).
[17] R. Pit, H. Hervet, and L. Leger, "Direct experimental evidence of slip in hexadecane: Solid interfaces," Phys. Rev. Lett. **85**, 980 (2000).
[18] D. C. Tretheway and C. D. Meinhart, "Apparent fluid slip at hydrophobic microchannel walls," Phys. Fluids **14**, L9 (2002).
[19] J.-L. Barrat and L. Bockquet, "Large slip effect at a nonwetting fluid–solid interface," Phys. Rev. Lett. **82**, 4671 (1999).
[20] J. Baudry, E. Charlaix, A. Tonck, and D. Mazuyer, "Experimental evidence for a large slip effect at a nonwetting fluid–surface interface," Langmuir **17**, 5232 (2001).
[21] Y. Zhu and S. Granick, "Limits of hydrodynamic no-slip boundary conditions," Phys. Rev. Lett. **88**, 106102 (2002).
[22] Y. Zhu and S. Granick, "Rate-dependent slip of Newtonian liquids at smooth surfaces," Phys. Rev. Lett. **87**, 096105 (2001).
[23] P. Attard, M. P. Moody, and J. W. G. Tyrrell, "Nanobubbles: The big picture," Physica A **314**, 696 (2002).
[24] K. Watanabe, T. Takayama, S. Ogata, and S. Isozaki, "Flow between two coaxial rotating cylinders with a highly water-repellent wall," AIChE J. **49**, 1956 (2003).
[25] J. R. Philip, "Flows satisfying mixed no-slip and no-shear conditions," Z. Angew. Math. Phys. **23**, 353 (1972).
[26] J. R. Philip, "Integral properties of flows satisfying mixed no-slip and no-shear conditions," Z. Angew. Math. Phys. **23**, 960 (1972).
[27] E. Lauga and H. A. Stone, "Effective slip in pressure driven Stokes flow," J. Fluid Mech. **489**, 55 (2003).
[28] R. Williams, *Modern GaAs Processing Methods* (Artech, Boston, 1990).
[29] M. Madau, *Fundamentals of Microfabrication* (CRC, Boca Raton, FL, 1997).
[30] J. C. McDonald, D. C. Duffy, J. R. Anderson, D. T. Chiu, H. Wu, O. J. A. Schueller, and G. M. Whitesides, "Fabrication of microfluidic systems in poly(dimethylsiloxane)," Electrophoresis **21**, 27 (2000).
[31] T.-R. Hsu, *MEMS & Microsystems: Design and Manufacture* (McGraw-Hill, Boston, MA, 2002).
[32] R. D. Blevins, *Applied Fluid Dynamics Handbook* (Van Nostrand Reinhold, New York, 1984).
[33] T. R. Corle and G. S. Kino, *Confocal Scannin Optical Microscopy and Related Imaging Systems* (Academic, San Diego, 1996).
[34] P. Kavehpour, B. Ovryn, and G. H. McKinley, "Evaporation-driven Marangoni instabilities of volatile liquid films spreading on thermally conductive substrates," Colloids Surf., A **206**, 409 (2002).
[35] F. P. Beer and E. R. Johnston, *Mechanics of Materials* (McGraw-Hill, New York, 1992).